Environment, Resource and Ecology Journal (2026)
Clausius Scientific Press, Canada

DOI: 10.23977/erej.2026.100107
ISSN 2616-3756 Vol. 10 Num. 1

Managing Asphaltene Flow Assurance in CO_2 Flooding: Molecular Guidance for Evaluating Operational Limits and Oil Chemistry

Peng Wang*

SINOPEC Petroleum Exploration & Production Research Institute, Beijing, 102206, China
wangpeng2022.syky@sinopec.com
**Corresponding Author*

Keywords: CO_2 flooding; asphaltene association; molecular dynamics simulation; non-covalent in-teractions; π-π stacking

Abstract: Asphaltene deposition remains a critical flow assurance challenge during CO_2 enhanced oil recovery (EOR), often causing abrupt injectivity decline and near-wellbore formation damage. While field experience indicates that pressure, temperature, and injection gas concentration control precipitation severity, a quantitative link between these operational parameters and crude oil molecular architecture is lacking. This study employs molecular dynamics (MD) simulations to bridge this gap, using a validated SARA-based crude oil model to systematically decouple the effects of operational variables (pressure, temperature, CO_2 concentration) from intrinsic molecular architecture (continental vs. archipelago asphaltenes). Results indicate that pressure depletion from 40 MPa to 10 MPa increases the asphaltene aggregate size by 24%, equivalent to a 58% increase in thermodynamic incompatibility (Δδ) with the oil phase. Furthermore, continental-type asphaltenes exhibit a 21.6% stronger self-association energy than archipelago types, suggesting that reservoirs rich in large aromatic cores possess a significantly narrower operational window for CO_2 injection before precipitation occurs. Crucially, this work translates molecular-scale non-covalent interactions into practical screening criteria: it identifies a critical Δδ threshold for deposition onset and highlights that controlling the CO_2 concentration below 20 mol% can suppress aggregate growth by approximately 33% compared to high-concentration floods. This molecular-to-engineering framework provides reservoir engineers with a mechanistic basis to pre-screen crude oil samples, tailor injection pressures to avoid the bubble-point region, and adjust CO_2 slug sizes to mitigate near-wellbore formation damage.

1. Introduction

CO_2 flooding has become a widely used EOR technique, valued for its ability to both improve oil recovery and enable geological CO_2 storage [1,2]. However, the injection of CO_2 disturbs the thermodynamic equilibrium of crude oil, often triggering asphaltene precipitation, flocculation, and subsequent deposition within reservoir pores [3,4]. Such deposition can block pore throats, alter rock

wettability, reduce permeability, and significantly impair gas injection efficiency and oil recovery [5,6]. Therefore, understanding the key factors that govern asphaltene deposition and their underlying microscopic mechanisms during CO_2 flooding is of considerable theoretical and engineering importance [7].

Asphaltenes are commonly defined as the fraction of petroleum that is insoluble in low molecular weight n-alkanes but soluble in aromatic solvents [8]. They typically exhibit high molecular weight, high polarity, and complex polyaromatic structures containing heteroatoms (N, O, S) and metals [9,10]. Based on the continuity of the aromatic core, asphaltene molecular models are generally divided into continental-type (island) and archipelago-type architectures [11,12]. In crude oil, asphaltenes exist in a colloidal state and are mainly stabilized by resins through peptization [13]. When external conditions change, asphaltene molecules associate via non-covalent interactions (e.g., π–π stacking, hydrogen bonding), forming nanoaggregates and larger clusters that may eventually precipitate [14,15]. The Yen–Mullins hierarchical model describes asphaltene aggregation at three levels: molecules, nanoaggregates, and clusters [12], while the supramolecular model emphasizes non-covalent interactions as the primary stabilizing forces [15].

Extensive experimental studies have investigated CO_2-induced asphaltene precipita-tion under various conditions. Key controlling parameters include pressure, temperature, CO_2 concentration, and oil composition [16–20]. Pressure is widely recognized as a dominant factor, with maximum precipitation typically occurring near the bubble point pressure [21,22]. Temperature effects appear to be oil-dependent: in light oils, increasing temperature tends to promote precipitation, whereas in heavy oils, it may stabilize asphaltenes [23–25]. CO_2 concentration exhibits a critical threshold beyond which precipitation increases sharply [17,18]; moreover, supercritical CO_2 can alter precipitation behavior owing to its unique physicochemical properties [26]. In porous media, asphaltene deposition can lead to permeability impairment and wettability alteration, with mechanisms involving surface adsorption, mechanical plugging, and entrainment [27–30]. Recent advances in experimental techniques have significantly deepened our understanding of these pore-scale phenomena. High-pressure microfluidic systems now enable direct visualization of asphaltene deposition dynamics within representative pore networks, revealing that deposition patterns are strongly influenced by flow rate, pore geometry, and the extent of CO_2 dissolution [31,32]. Low-field nuclear magnetic resonance (NMR) has also emerged as a powerful tool for in-situ monitoring of pore blockage and wettability evolution during CO_2 flooding, providing quantitative relationships between asphaltene saturation and permeability reduction [28,33]. Despite these technological advances, a systematic integration of pore-scale observations with molecular-level interaction mechanisms remains elusive.

Various thermodynamic models have been developed to describe asphaltene precipitation, including solubility models based on Flory–Huggins theory [34,35], colloidal models [5], and equation-of-state (EOS) approaches such as Perturbed-Chain Statistical Associating Fluid Theory (PC-SAFT) and Cubic-Plus-Association (CPA) [36–39]. Machine learning methods have also been applied to predict precipitation parameters, demonstrating notable accuracy when trained on extensive experimental datasets [16,40,41]. However, these macroscopic models inherently lack molecular specificity and cannot elucidate how specific intermolecular forces dictate aggregation pathways. MD simulation provides a powerful means to address this gap by enabling direct observation of asphaltene aggregation at the atomistic scale [42,43]. Despite these important contributions, the majority of MD investigations have been conducted under idealized conditions that do not fully capture the compositional complexity of real crude oils, and more critically, they have not been systematically coupled with statistical analyses of experimental or field data. While previous works have separately performed statistical assessments of precipitation risk factors [16] and MD-based aggregation simulations, no study to date has quantitatively linked macroscopic controlling

parameters—derived from comprehensive experimental datasets—to the corresponding molecular interaction fingerprints revealed by MD. This disconnect impedes the development of predictive frameworks that bridge scales from molecular aggregation to reservoir-scale deposition.

To address this gap, a molecular model of crude oil based on SARA fractions is con-structed. MD simulations are carried out to systematically investigate the effects of thermodynamic conditions (pressure, temperature, CO_2 concentration) and molecular structure (molecular type, heteroatoms, aromatic core size) on asphaltene association behavior. The findings are expected to offer theoretical guidance for predicting asphaltene deposition risks and optimizing CO_2 flooding parameters, while demonstrating the value of integrating molecular simulation with statistical data analytics for complex multiphase flow problems.

2. Methods

2.1. Model Construction

A crude oil molecular model was built following the SARA (saturates, aromatics, resins, asphaltenes) fractionation approach. Representative molecular monomers were selected to capture the chemical diversity of crude oil components. For saturates, n-eicosane ($C_{20}H_{42}$) was used to represent long-chain alkanes. Phenanthrene ($C_{14}H_{10}$) was chosen as the aromatic component because its fused-ring structure is typical of petroleum aromatics. A sulfur- and oxygen-containing fused-ring aromatic derivative was employed to represent the resin fraction, reflecting the heteroatom functionality characteristic of this class. For asphaltenes, two common molecular architectures were incorporated: the continental (island) type, which features a single large fused aromatic core, and the archipelago type, consisting of several smaller aromatic cores linked by alkyl chains. The molecular geometries are shown in Fig. 1. All molecules were randomly packed into a cubic simulation box of 10 nm×10 nm×10 nm using Packmol, ensuring a loose initial configuration free of atomic overlaps. Periodic boundary conditions were applied in all three dimensions to mimic an infinite bulk system.

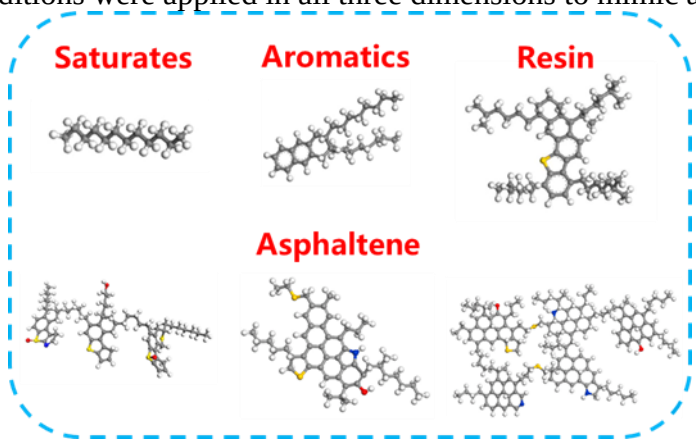

Figure 1: Molecular configuration of hydrocarbon molecules in crude oil.

2.2. Force Field and Simulation Parameters

Intermolecular interactions among hydrocarbon molecules were described using the CVFF force field, which is based on the Lennard-Jones 12-6 potential and is known to reliably predict structures and binding energies of organic molecules. CO_2 was modeled with the EPM2 force field, which accurately reproduces the thermodynamic and transport properties of CO_2 under reservoir conditions. Non-bonded van der Waals interactions were truncated at 10 Å, and electrostatic interactions were truncated at 15 Å. Long–range electrostatic interactions were handled using the particle–particle–

particle–mesh (PPPM) algorithm, which provides efficient and accurate treatment of Coulombic forces in periodic systems. A tail correction was applied to account for long-range van der Waals interactions beyond the cutoff distance, improving the accuracy of energy and pressure calculations.

2.3. Simulation Protocol

All molecular dynamics simulations were carried out with the LAMMPS package, a widely used open-source code for large-scale atomic and molecular simulations. Energy minimization was first performed in the canonical (NVT) ensemble using the conjugate gradient method to eliminate unfavorable atomic contacts and obtain a low-energy starting configuration. The system was then heated from 300 K to 1000 K and equilibrated at 1000 K for 500 ps in the NVT ensemble to allow full molecular relaxation, ensuring that all molecules could overcome energy barriers and thoroughly explore configurational space. The ensemble was then switched to isothermal–isobaric (NPT), and the system was further equilibrated at 1000 K and 40 MPa for an additional 500 ps. An annealing process was subsequently carried out in the NPT ensemble by stepwise cooling and depressurization: the temperature was reduced in stages to 800 K, 600 K, 400 K, and finally 338 K, while the pressure was decreased to 20 MPa to reach typical reservoir conditions. Each stage lasted 500 ps with a time step of 1 fs. This annealing protocol was designed to gradually bring the system from a well-relaxed high-temperature state to realistic reservoir conditions while avoiding kinetic trapping. The final equilibrated configuration under reservoir conditions is shown in Fig. 2.

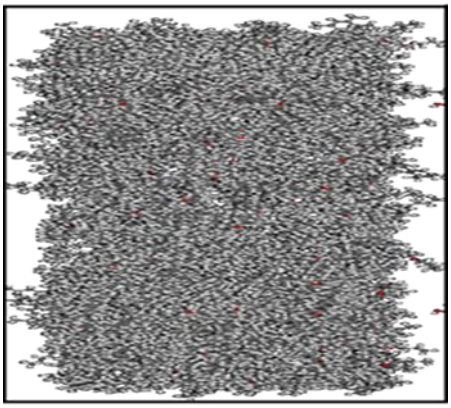

Figure 2: Hydrocarbon components model of the crude oil.

3. Results

3.1. Effects of Thermodynamic Conditions on Asphaltene Association

To systematically investigate how pressure, temperature, and CO_2 concentration influence asphaltene association, this section adopts a consistent analytical framework based on the interaction energy, radius of gyration, and solubility parameter. Each thermodynamic factor is examined in turn using this set of descriptors to ensure structural coherence and mechanistic clarity.

3.1.1. Pressure Effect

The interaction energy analysis (Fig. 3) provides quantitative support for this picture. Taking 60 °C as a representative condition, reducing pressure from 40 MPa to 10 MPa shifts the average asphaltene–asphaltene interaction energy from -15855 kcal/mol to -15888 kcal/mol—an increase in absolute magnitude of 33 kcal/mol. Although this corresponds to a modest relative rise of about 0.21%, it still represents a non-negligible gain in attractive energy at the molecular level. More

importantly, the same monotonic trend is observed across all temperatures examined (20 °C to 80 °C): lower pressure consistently gives more negative (i.e., more attractive) interaction energies. The pressure sensitivity is strongest in the range from 30 MPa down to 10 MPa, with an average increase of roughly 1.65 kcal/mol per 1 MPa decrease. Van der Waals contributions dominate over electrostatic terms. Taken together, these results confirm that lowering pressure directly strengthens cohesive interactions among asphaltenes, thus encouraging the growth of larger and more stable nanoaggregates.

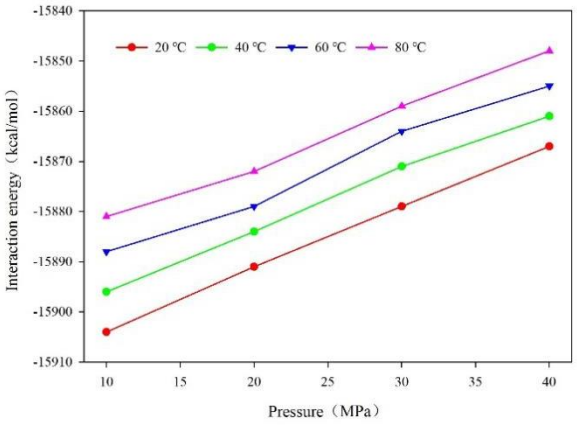

Figure 3: The interaction energy curves of asphaltene molecules under different pressures and temperatures.

Meanwhile, the radius of gyration (R_g) of asphaltene aggregates (Fig. 4) increases from 98.0 Å at 40 MPa to 121.5 Å at 10 MPa, a 24.0% increase (23.5 Å absolute). The pressure-sensitivity is non-linear, with the steepest rise occurring between 30 MPa and 20 MPa (R_g: 102 Å→116 Å). The R_g distribution also broadens at low pressure, reflecting the co-existence of small and large clusters—a signature of enhanced aggregation kinetics. These results quantitatively support the conclusion that reduced pressure promotes larger and more polydisperse asphaltene aggregates.

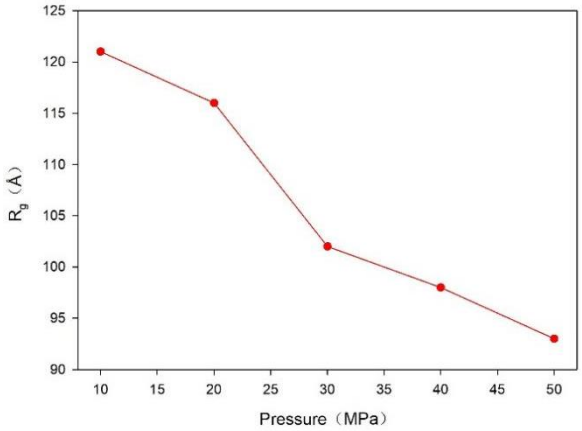

Figure 4: The radius of gyration (Rg) curves of asphaltene aggregates under different pressures.

The solubility parameter difference between asphaltenes and the crude oil (Fig. 5) provides a thermodynamic rationale. As pressure decreases from 40 MPa to 10 MPa, the solubility parameter of the crude oil decreases from 15.6 $(MPa)^{0.5}$ to 12.08 $(MPa)^{0.5}$, while that of asphaltenes remains nearly constant. Consequently, the difference $\Delta\delta$ increases from 5.15 $(MPa)^{0.5}$ to 8.12 $(MPa)^{0.5}$ – a 58% increase. According to regular solution theory, a larger $\Delta\delta$ implies stronger incompatibility and a higher thermodynamic driving force for asphaltene phase separation. Thus, pressure reduction promotes aggregation not only by enhancing intermolecular attractions but also by worsening the

solubility match between asphaltenes and the oil medium.

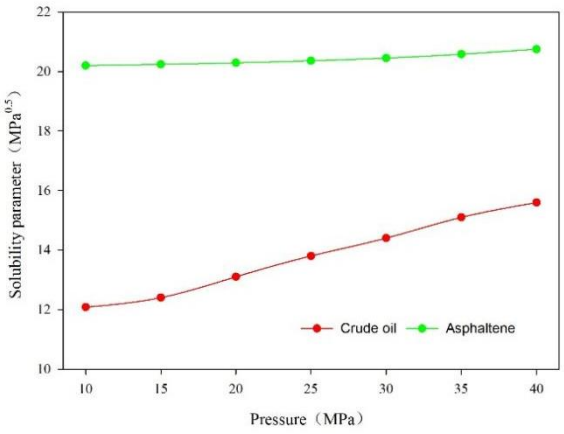

Figure 5: The solubility parameter curves under different pressures.

The 24% increase in aggregate radius when pressure drops from 40 MPa to 10 MPa suggests a critical operational threshold. To mitigate severe near-wellbore deposition, it is advisable to maintain bottomhole flowing pressure above the bubble point and above 30 MPa whenever feasible. If pressure depletion is unavoidable (e.g., in mature floods), operators should anticipate a sharp rise in asphaltene instability and consider preemptive solvent squeezes or inhibitor treatments as pressure approaches 20 MPa.

3.1.2. Temperature Effect

The interaction energy data (Fig. 3) show that at constant pressure (20 MPa), raising the temperature from 20 ℃ to 80 ℃ reduces the asphaltene–asphaltene interaction energy from -15891 kcal/mol to -15872 kcal/mol – an absolute decrease of 19 kcal/mol in magnitude. The temperature sensitivity is particularly pronounced for hydrogen bonding contributions, which drop by nearly 50%, while π-π stacking contributions decrease by about 25%. This differential response reflects the fact that hydrogen bonds are more easily broken by thermal agitation than the more distributed π-π interactions. Consequently, aggregates partially disintegrate into smaller units, as evidenced by the decrease in R_g from 106.1 Å at 20 ℃ to 80 Å at 100 ℃ (Fig. 6). The R_g distribution becomes narrower and shifts toward lower values, consistent with a more homogeneous population of small aggregates.

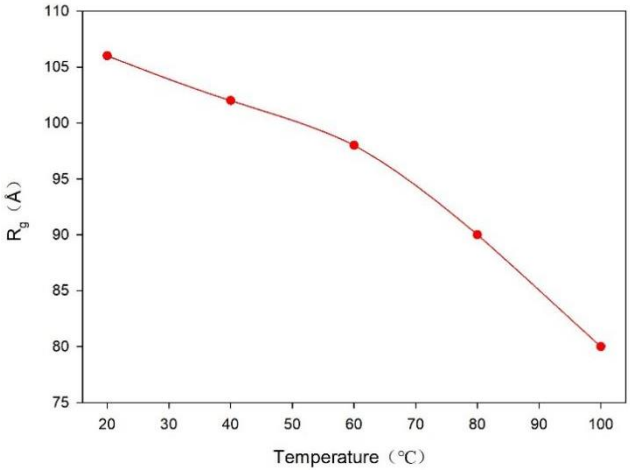

Figure 6: The radius of gyration (R_g) curves of asphaltene aggregates under different temperatures.

The solubility parameter analysis (Fig. 7) further clarifies the temperature effect. As temperature increases from 20 ℃ to 80 ℃, the solubility parameter of the crude oil decreases slightly from 15.80 $(MPa)^{0.5}$ to 15.45 $(MPa)^{0.5}$, while that of asphaltenes decreases more substantially from 22.27 $(MPa)^{0.5}$ to 20.12 $(MPa)^{0.5}$. Consequently, the difference $\Delta\delta$ (asphaltene minus oil) drops from 6.47 $(MPa)^{0.5}$ to 4.67 $(MPa)^{0.5}$ – a relative reduction of approximately 28%. This improved compatibility at higher temperatures lowers the thermodynamic driving force for phase separation, explaining why asphaltene deposition risk is generally lower in high-temperature reservoirs. Notably, the dominant contribution to the reduced $\Delta\delta$ comes from the temperature-induced decline in asphaltene solubility parameter, rather than from changes in the oil phase. However, it should be noted that in some heavy oils, temperature may also reduce oil viscosity and promote asphaltene diffusion, leading to a more complex, non-monotonic behavior – a nuance that depends on the specific crude oil composition.

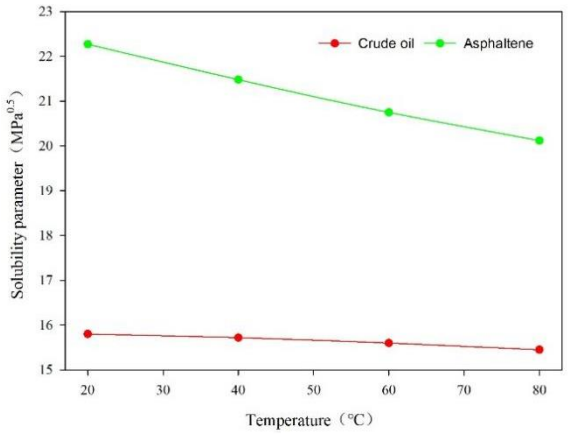

Figure 7: The solubility parameter curves under different temperatures.

3.1.3. CO_2 Concentration Effect

The radius of gyration (Fig. 8) increases markedly with CO_2 concentration: from 98.0 Å at 0% CO_2 to 130.0 Å at 40% CO_2, representing a 32.7% increase in aggregate size. Moreover, the R_g distribution becomes bimodal at high CO_2 concentrations, suggesting the coexistence of small nanoaggregates and large clusters – a precursor to macroscopic precipitation. These results quantitatively confirm that CO_2 injection promotes the growth of asphaltene aggregates.

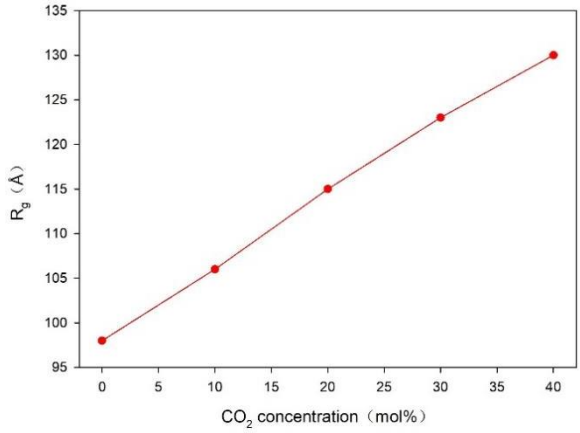

Figure 8: The radius of gyration curves under different CO_2 concentrations.

The solubility parameter difference (Fig. 9) widens progressively with increasing CO_2 concentration: $\Delta\delta$ increases from 5.15 $(MPa)^{0.5}$ without CO_2 to 6.13 $(MPa)^{0.5}$ at 40 mol% CO_2 – a

relative increase of approximately 19% over the range 0–40 mol%. This growing mismatch indicates that the crude oil becomes a poorer solvent for asphaltenes, driving enhanced aggregation and eventual deposition. It is worth noting that supercritical CO_2, which was used in this study (reservoir conditions of 338 K and 20 MPa are above the critical point of CO_2, $T_c = 304$ K, $P_c = 7.38$ MPa), exhibits near-zero surface tension and high diffusivity, allowing it to penetrate asphaltene nanoaggregates and further disrupt the solvation shell. This explains why CO_2 flooding often causes more severe asphaltene problems compared to other gases.

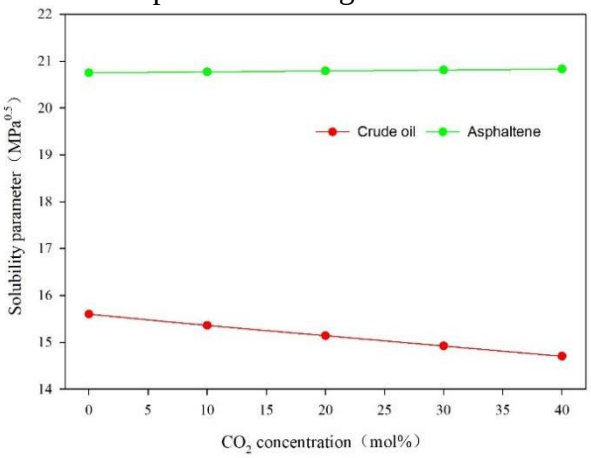

Figure 9: The solubility parameter curves under different CO_2 concentrations.

The bimodal aggregate distribution observed at 40 mol% CO_2 indicates the coexistence of stable nanoaggregates and precipitating clusters, a precursor to pore plugging. This finding supports the use of Water-Alternating-Gas (WAG) injection schemes. By reducing the in-situ CO_2 saturation and limiting the local concentration below 20–30 mol%, WAG can effectively suppress the formation of the large, problematic clusters identified in these simulations.

3.2. Effects of Molecular Structure on Asphaltene Association

While thermodynamic conditions modulate the external environment, the intrinsic aggregation propensity of asphaltenes is governed by their molecular architecture, heteroatom functionality, and compositional polydispersity. This section applies the same analytical framework—interaction energy, R_g, and δ—to systematically examine these structure–property relationships.

3.2.1. Effect of Aromatic Core Size and Molecular Architecture

The interaction energy (Fig. 10) quantifies the difference in aggregation strength: the asphaltene–asphaltene interaction energy for continental molecules is -12461.0 kcal/mol, compared to -10251.0 kcal/mol for archipelago molecules — a 21.6% increase in attractive energy. This significant enhancement reflects the stronger π–π stacking facilitated by the extended aromatic core in the continental structure. While the absolute energy values depend on system size and simulation protocol, the relative difference underscores the thermodynamic favorability of continental asphaltene aggregation. The van der Waals contribution, dominated by π–π interactions, remains the primary driver of this difference.

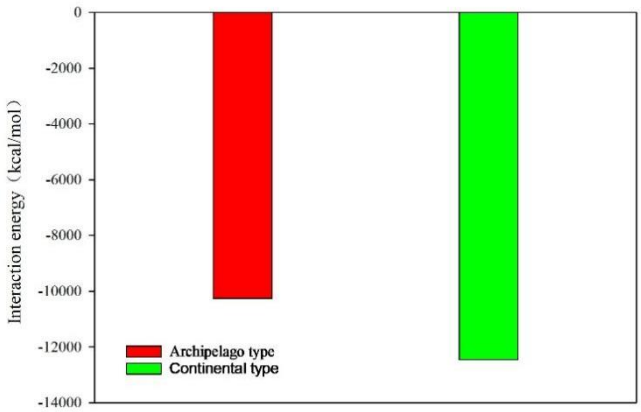

Figure 10: The interaction energy curves of asphaltene molecules under different molecular architecture.

Consequently, continental asphaltenes form larger aggregates, as reflected in their radius of gyration (Fig. 11). Based on the simulation data, the R_g value for continental asphaltenes is 119.0 Å, whereas archipelago asphaltenes exhibit a value of 102.0 Å—a 16.7% increase. This trend confirms that the stronger π–π stacking in continental molecules promotes the formation of more extended aggregate structures.

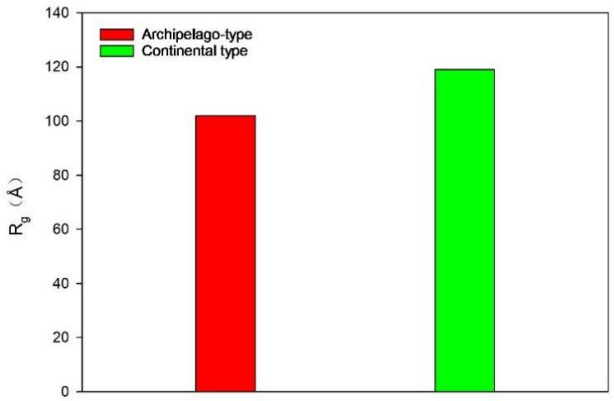

Figure 11: The radius of gyration curves of asphaltene molecules under different molecular architecture.

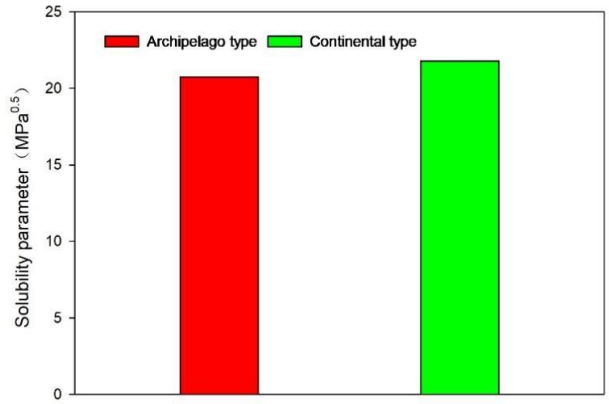

Figure 12: The solubility parameter curves of asphaltene molecules under different molecular architecture.

The solubility parameter (Fig. 12) is also higher for continental asphaltenes: 21.79 $(MPa)^{0.5}$ compared to 20.75 $(MPa)^{0.5}$ for archipelago asphaltenes. It indicates that continental asphaltenes are inherently less compatible with the surrounding oil medium. Consequently, they exhibit a greater thermodynamic driving force to precipitate when the solvent quality deteriorates—for instance, during CO_2 injection or pressure depletion.

From a mechanistic perspective, the large aromatic core of continental asphaltenes promotes a face-to-face stacking geometry with interplanar distances of 3.5–4.0 Å, optimized for π-π interactions. In contrast, archipelago asphaltenes tend to aggregate via edge-to-face or T-shaped configurations, which are weaker. Moreover, the flexible alkyl linkers between small aromatic units in archipelago structures introduce conformational entropy that partially opposes association. These molecular-scale differences directly translate into macroscopic deposition risk: reservoirs containing predominantly continental asphaltenes are inherently more vulnerable.

The significant disparity in interaction energy (-12461 vs. -10251 kcal/mol) between continental and archipelago asphaltenes translates to a predictable difference in field deposition risk. Crude oils with a high proportion of continental asphaltenes (indicated by high aromaticity in SARA analysis or low H/C ratio) should be flagged as high-risk for CO_2 EOR projects. For such oils, more conservative injection strategies, lower initial CO_2 slug sizes, or the inclusion of aromatic solvents in the injection stream should be evaluated during the laboratory screening phase.

3.2.2. Effect of Heteroatoms and Functional Groups

The hydrogen bond count (Fig. 13) reveals a striking reversal of the expected trend: archipelago asphaltenes with oxygen functional groups exhibit a significantly higher number of hydrogen bonds (plateauing at ≈11-12 in the aggregated state) compared to continental asphaltenes (plateauing at ≈1.1). This counterintuitive result suggests that the flexible, multi-core architecture of archipelago molecules allows greater exposure and accessibility of polar functional groups, thereby facilitating more extensive hydrogen-bond networks despite weaker π–π stacking. These hydrogen bonds act as "molecular stitches", enhancing cohesion energy and promoting the formation of stable, albeit structurally looser, clusters in archipelago systems.

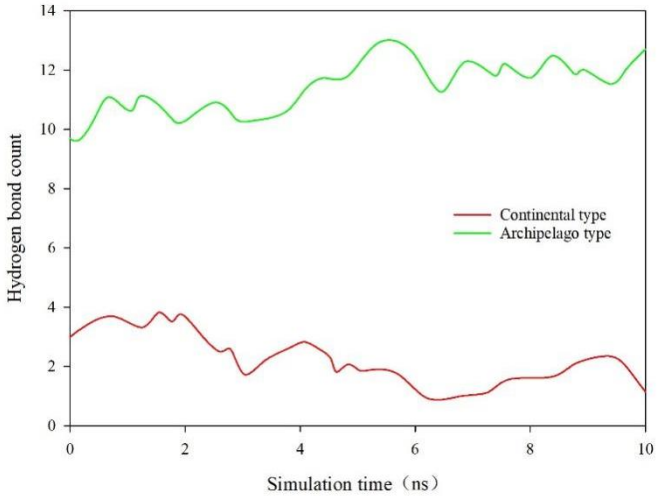

Figure 13: The hydrogen bond count of asphaltene molecules under different molecular architecture.

3.2.3. Effect of Polydispersity

Real asphaltenes are not monodisperse; they consist of a wide range of molecular weights and

architectures. The radius of gyration values (Fig. 14) obtained from simulations illustrate this structural diversity: pure archipelago asphaltenes exhibit an R_g of 102.0 Å, continental asphaltenes reach 119.0 Å, and a mixed system of both architectures yields an intermediate value of 116.0 Å. This ordering confirms that continental molecules, with their larger aromatic cores, form more extended aggregates, and that the presence of continental components in a polydisperse mixture enlarges the overall aggregate dimensions. This polydispersity leads to complex, staged aggregation behavior: smaller, more soluble asphaltene molecules may remain dispersed while larger, more aromatic ones precipitate first.

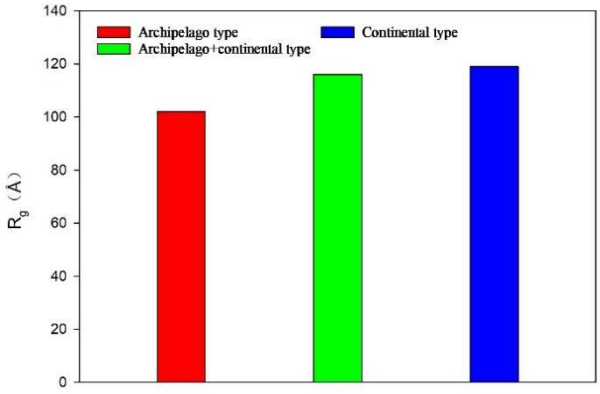

Figure 14: The radius of gyration curves of asphaltene molecules with polydispersity.

The solubility parameter (δ) reflects the cohesive energy density of asphaltene molecules and their compatibility with the surrounding oil medium. As shown in Fig. 15, archipelago-type asphaltenes have the lowest solubility parameter, at 20.75 $(MPa)^{0.5}$, while continental-type asphaltenes show the highest value, 21.64 $(MPa)^{0.5}$. A mixed system containing both architectures gives an intermediate δ of 21.58 $(MPa)^{0.5}$. Although these differences appear small numerically, they carry thermodynamic significance: the higher δ of continental asphaltenes indicates stronger self-association and poorer compatibility with the maltene phase, making them inherently more prone to phase separation. The intermediate value seen in the mixed system suggests that blending different molecular architectures moderates the overall cohesive energy, which may in turn affect the aggregation pathway and precipitation behavior of polydisperse asphaltene samples.

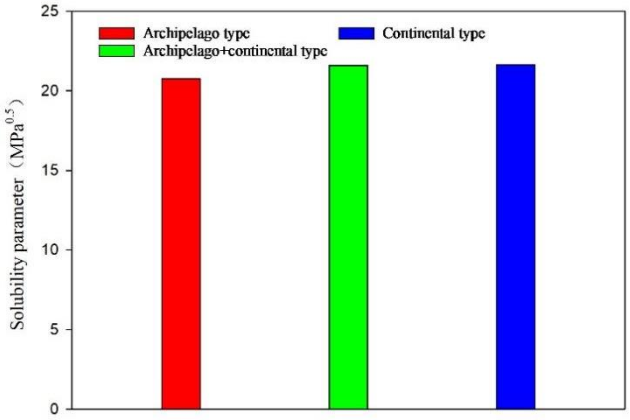

Figure 15: The solubility parameter curves of asphaltene molecules with polydispersity.

The practical implication is that deposition does not occur as a single event but rather as a progressive process: initial precipitation of the most incompatible asphaltene fractions may plug pore throats, followed by later deposition of less incompatible fractions, potentially exacerbating

formation damage. From a modeling perspective, representing asphaltenes as a single average molecule is insufficient; a distribution of structures is necessary to capture the onset and extent of deposition accurately.

4. Discussion

Building on the quantitative trends established in Section 3, we synthesize the findings into an operational risk matrix for CO_2 flooding. The matrix integrates three tiers of control:

(1) Primary Drivers (Non-covalent interactions): π-π stacking (60–70% of binding energy) dictates baseline aggregation strength.

(2) External Regulators (Operational Levers): Pressure and CO_2 concentration are the most potent levers available to field engineers for modulating the solubility mismatch (Δδ).

(3) Intrinsic Determinants (Crude Oil Fingerprint): The continental vs. archipelago character of the asphaltene fraction sets the inherent susceptibility of the oil.

This framework allows for a tiered risk assessment. Tier 1 involves a simple SARA or spectroscopic analysis to determine if the crude is "continental-type" (high risk) or "archipelago-type" (moderate risk). Tier 2 involves applying the pressure and CO_2 concentration limits derived from this simulation (e.g., $P > 30$ MPa, $CO_2 < 20\%$) to define a safe injection envelope for that specific oil.

The practical implications for CO_2 flooding design are clear: reservoirs with high asphaltene content and continental-type molecular structures require more cautious injection strategies—such as lower injection pressures, temperature management, or water-alternating-gas schemes—to mitigate the solubility parameter disparity and prevent severe deposition.

5. Conclusions

This study combines MD simulations with a systematic examination of thermodynamic and structural variables to uncover the microscopic mechanisms that govern asphaltene association during CO_2 flooding. The main findings are summarized below:

(1) The aggregation driving force is dominated by non-covalent interactions, primarily π-π stacking, which accounts for 60–70% of the cohesive energy. This implies that crude oils with extended aromatic cores (continental-type) possess an inherently higher baseline risk for deposition during CO_2 injection, regardless of operational care.

(2) Pressure depletion below 30 MPa and CO_2 concentrations exceeding 20 mol% were identified as critical destabilization thresholds. Exceeding these limits triggers a 24-33% growth in aggregate size and a 58% increase in thermodynamic incompatibility (Δδ). Maintaining reservoir conditions above these thresholds is recommended to avoid the steep rise in aggregation propensity observed near the bubble point.

(3) Molecular architecture is a decisive intrinsic factor. Continental-type asphaltenes, with their extended aromatic cores, demonstrate a markedly higher aggregation propensity and form larger clusters ($R_g \approx 119.0$ Å) compared to archipelago-type molecules ($R_g \approx 102.0$ Å). The greater thermodynamic incompatibility of continental structures renders reservoirs rich in these components inherently more susceptible to deposition during CO_2 flooding.

(4) An operational framework is proposed based on the molecular simulation results. This framework utilizes crude oil molecular architecture (continental vs. archipelago) as a primary risk indicator and translates the simulation-derived pressure and CO_2 concentration sensitivities into practical guidance for defining the safe operating envelope of CO_2 EOR projects.

Acknowledgement

This research was funded by "SINOPEC Technology Department Young Doctoral Support Program, grant number P25148".

References

[1] Green DW, Willhite GP. Enhanced Oil Recovery. Richardson, TX, USA: Society of Petroleum Engineers; 1998.
[2] Donaldson EC, Chilingarian GV, Yen TF. Enhanced Oil Recovery, II: Processes and Operations. Amsterdam, The Netherlands: Elsevier; 1989.
[3] Burke NE, Hobbs RE, Kashou SF. Measurement and modeling of asphaltene precipitation. J Pet Technol. 1990;42(11):1440–1446. doi:10.2118/18273-PA
[4] Cao M, Gu Y. Temperature effects on the phase behaviour, mutual interactions and oil recovery of a light crude oil–CO_2 system. Fluid Phase Equilib. 2013;356:78–89. doi:10.1016/j.fluid.2013.07.006
[5] Leontaritis KJ, Mansoori GA. Asphaltene deposition: a survey of field experiences and research approaches. J Pet Sci Eng. 1988;1(3):229–239. doi:10.1016/0920-4105(88)90013-7
[6] Eskin D, Mohammadzadeh O, Akbarzadeh K, Taylor SD, Ratulowski J. Reservoir impairment by asphaltenes: a critical review. Can J Chem Eng. 2016;94(7):1202–1217. doi:10.1002/cjce.22476
[7] Tazikeh S, Mohammadzadeh O, Zendehboudi S. Characterization and multiphase flow of Oil/ CO_2 systems in porous media focusing on asphaltene precipitation: a systematic review. Geoenergy Sci Eng. 2025;247:213554. doi:10.1016/j.geoen.2024.213554
[8] Speight JG. The Chemistry and Technology of Petroleum. 4th ed. Boca Raton, FL, USA: CRC Press; 2006.
[9] Seifried CM. Asphaltene Deposition in Porous Media. Lyngby, Denmark: Technical University of Denmark; 2016.
[10] Kelland MA. Production Chemicals for the Oil and Gas Industry. 3rd ed. Boca Raton, FL, USA: CRC Press; 2016.
[11] Ghamartale A, Rezaei N, Zendehboudi S. Alternation of asphaltene binding arrangement in the presence of chemical inhibitors: molecular dynamics simulation strategy. Fuel. 2023;336:127001. doi:10.1016/j.fuel.2022.127001
[12] Mullins OC. The modified Yen model. Energy Fuels. 2010;24(4):2179–2207. doi:10.1021/ef900975e
[13] Asomaning S. Test methods for determining asphaltene stability in crude oils. Pet Sci Technol. 2003;21(3-4):581–590. doi:10.1081/LFT-120018540
[14] Yen TF, Chilingarian GV. Asphaltenes and Asphalts. Vol. 1. Amsterdam, The Netherlands: Elsevier; 1994.
[15] Gray MR, Tykwinski RR, Stryker JM, Tan X. Supramolecular assembly of asphaltenes. Energy Fuels. 2011;25(7):3125–3134. doi:10.1021/ef200654p
[16] Zendehboudi S, Ahmadi MA, Mohammadzadeh O, Bahadori A, Chatzis I. Thermodynamic investigation of asphaltene precipitation during CO_2 injection. Fuel. 2014;117(Pt A):259–268. doi:10.1016/j.fuel.2013.09.052
[17] Yang Z, Ma C, Lin M, Dong Z. Experimental study on asphaltene precipitation during CO_2 injection. J Can Pet Technol. 1999;38(13):38–42. doi:10.2118/99-13-04
[18] Alizadeh A, Nakhli H, Kharrat R, Ghazanfari M, Aghajani M. Experimental study of asphaltene precipitation behavior during miscible carbon dioxide injection. Energy Sources Part A. 2014;36(14):1523–1530. doi:10.1080/15567036.2011.551921
[19] Wang X, Gu Y. Experimental study of asphaltene precipitation during CO_2 flooding. Energy Fuels. 2011;25(4):1591–1601. doi:10.1021/ef200037x
[20] Elturki M, Imqam A. An experimental investigation of asphaltene aggregation under carbon dioxide injection flow in ultra-low-permeability pore structure. In: Proceedings of the SPE Canadian Energy Technology Conference; 2022 Mar 16–17; Calgary, AB, Canada. SPE-208802-MS. doi:10.2118/208802-MS
[21] Hussein A. Asphaltene deposition. In: Hussein A, editor. Essentials of Flow Assurance Solids in Oil and Gas Operations. Oxford, UK: Gulf Professional Publishing; 2023. p. 377–427.
[22] Ru H, Alta'ee AF. Asphaltene precipitation during CO_2 injection. J Pet Sci Eng. 2015;127:1–8. doi:10.1016/j.petrol.2015.01.013
[23] Monger TG, Fu JC. The nature of CO_2-induced organic deposition. In: Proceedings of the SPE Annual Technical Conference and Exhibition; 1987 Sep 27–30; Dallas, TX, USA. SPE-16713-MS. doi:10.2118/16713-MS
[24] Fakher S, Adaya M, Elturki M, Imqam A. An experimental investigation of asphaltene stability in heavy crude oil during carbon dioxide injection. J Pet Explor Prod Technol. 2020;10(3):919–931. doi:10.1007/s13202-019-00782-7
[25] Fakher S, Imqam A. An experimental investigation of immiscible carbon dioxide interactions with crude oil: oil swelling and asphaltene agitation. Fuel. 2020;269:117380. doi:10.1016/j.fuel.2020.117380
[26] Cruz AA, Amaral M, Santos D, Palma A, Franceschi E, Santos AF, et al. CO_2 influence on asphaltene precipitation. J Supercrit Fluids. 2019;143:24–31. doi:10.1016/j.supflu.2018.08.007
[27] Soroush S, Pourafshary P, Vafaie-Sefti M. A comparison of asphaltene deposition in miscible and immiscible CO_2

flooding. Pet Sci Technol. 2014;32(15):1824–1832. doi:10.1080/10916466.2012.744880
[28] Huang Y, Zhang X, Liu W, Wang Z. Investigation of asphaltene precipitation in tight oil reservoirs during CO_2 huff-n-puff. Fuel. 2023;312:122943. doi:10.1016/j.fuel.2021.122943
[29] Wang Z, Li Y, Zhang H, Chen X. Evaluation of asphaltene precipitation during CO_2 flooding in tight oil reservoirs. Energy Fuels. 2022;36(16):8876–8887. doi:10.1021/acs.energyfuels.2c01127
[30] Tavakkoli M. Asphaltene Deposition in Porous Media: Experimental and Modeling Studies. Houston, TX, USA: Rice University; 2017.
[31] Mahdavifar M, Roozshanes AA, Miri R. Microfluidic experiments and numerical modeling of pore-scale asphaltene deposition: insights and predictive capabilities. Energy. 2023;283:129210. doi:10.1016/j.energy.2023.129210
[32] Betancur S, Quevedo L, Olmos CM. Microfluidic devices, materials, and recent progress for petroleum applications: a review. Can J Chem Eng. 2024;102(7):2583–2607. doi:10.1002/cjce.25234
[33] Morgan VG, Barbosa LL, Lacerda V, de Castro EVR. Application of low-field nuclear magnetic resonance to assess the onset of asphaltene precipitation in petroleum. Fuel. 2020;265:116955. doi:10.1016/j.fuel.2019.116955
[34] Hirschberg A, de Jong LNJ, Schipper BA, Meijer JG. Influence of temperature and pressure on asphaltene flocculation. SPE J. 1984;24(3):283–293. doi:10.2118/11202-PA
[35] Cimino R, Correra S, Sacomani P, Carminati C. Thermodynamic modelling for prediction of asphaltene deposition in live oils. In: Proceedings of the SPE International Symposium on Oilfield Chemistry; 1995 Feb 14–17; San Antonio, TX, USA. SPE-28993-MS. doi:10.2118/28993-MS
[36] Gonzalez DL, Ting PD, Hirasaki GJ, Chapman WG. Prediction of asphaltene instability under gas injection with the PC-SAFT equation of state. Energy Fuels. 2005;19(4):1230–1234. doi:10.1021/ef049782y
[37] Gross J, Sadowski G. Perturbed-chain SAFT: an equation of state based on a perturbation theory for chain molecules. Ind Eng Chem Res. 2001;40(4):1244–1260. doi:10.1021/ie0003887
[38] Panuganti SR, Vargas FM, Gonzalez DL, Kurup AS, Chapman WG. PC-SAFT modeling of asphaltene phase behavior. Energy Fuels. 2012;26(5):2528–2540. doi:10.1021/ef3001048
[39] Li Z, Firoozabadi A. Cubic-plus-association equation of state for asphaltene precipitation in live oils. Energy Fuels. 2010;24(5):2956–2963. doi:10.1021/ef9014263
[40] Khamehchi E, Behvandi R, Rashidi F. Prediction of bubble point pressure and asphaltene onset pressure during CO_2 injection using ANN and ANFIS models. In: Proceedings of the SPE Middle East Oil and Gas Show and Conference; 2011 Sep 25–28; Manama, Bahrain. SPE-143250-MS. doi:10.2118/143250-MS
[41] Mazloom MS, Hemmati-Sarapardeh A, Husein MM, Zendehboudi S. Artificial intelligence based methods for asphaltenes adsorption by nanocomposites: application of group method of data handling, least squares support vector machine, and artificial neural networks. Nanomaterials. 2020;10(5):890. doi:10.3390/nano10050890
[42] Diallo MS, Cagin T, Faulon JL, Goddard WA. Thermodynamic properties of asphaltenes: a predictive approach based on computer assisted structure elucidation and atomistic simulations. Dev Pet Sci. 2000;40:103–127. doi:10.1016/S0376-7361(00)80009-7
[43] Ghamartale A, Zendehboudi S, Mohamadi-Baghmolaei M. Control of asphaltene deposition by chemical inhibitors in calcite pore: molecular dynamics approach. Ind Eng Chem Res. 2022;61(31):11555–11567. doi:10.1021/acs.iecr.2c01568